Compression of the multiple ion-acoustic soliton at the bottom of the space potential

T. Nagasawa and Y. Nishida
Department of Electrical and Electronic Engineering, Utsunomiya University, Utsunomiya, Tochigi 321, Japan
(Received 2 June 1997)

Detailed experimental investigations on compressive phenomena are performed using a double-plasma-type device. When the incident multiple ion-acoustic soliton propagates to the ion-sheath edge, which is produced by the biased reflector to deep negative potential, this multiple soliton is compressed by the accelerated velocities of the second and third pulses and becomes a single soliton at the reflection point. It then resumes the form of a multiple soliton, as if via a recurrence phenomenon, and each pulse of this multiple soliton propagates toward the reflector. These phenomena are caused by an uneven space potential, which in turn is produced by deep negative voltage on the reflector and ion wakefield. Also, the reflection soliton is produced at this reflection point. [S1063-651X(97)01910-7]

PACS number(s): 52.35.Sb, 52.35.Mw

I. INTRODUCTION

Many phenomena of solitons have been extensively studied both theoretically and experimentally by a number of authors. Zabusky and Kruskal [1] have pointed out the recurrence of the Korteweg–de Vries (KdV) soliton by numerical calculation. Ikezi [2] and Watanabe, Ishihara, and Tanaka [3] have shown experimentally the recurrence of the ion-acoustic soliton using a double-plasma device.

Nishida, Nagasawa, and Kawamata have shown experimentally that the initial ion-acoustic cylindrical soliton passes through the cylindrical plasma column with strong interactions and without losing its identity [4,5], and that two plane ion-acoustic solitons resume the initial soliton shape [6,7] after the resonant interaction of their solitons. The phenomena of the reflection and/or transmission of the plane ion-acoustic soliton at a plasma boundary has also been investigated, both experimentally [8–15] and theoretically [16–19]. Nagasawa and Nishida [20] have shown that the reflection and refraction of two-dimensional solitons comply with nonlinear Snell's law. Nishida, Yoshida, and Nagasawa [21,22] have pointed out experimentally that the soliton tunnels through the sheath area without time delay, and that it is resonantly absorbed near the sheath area at $D \cong L$, where D is the spatial width of the incident soliton and L is the characteristic length of the sheath, e.g., a scale length of a density gradient in front of the reflector. Using inverse scattering, Matsuoka and Yajima [19] have shown theoretically that the reflection and refraction coefficients of two-dimensional shallow water solitons depend on the velocity ratio of the refraction and incident solitons. Nagasawa and Nishida [23–25] have shown that the experimental results of the reflection and/or refraction coefficients of the single plane soliton at the plasma boundary are in reasonable agreement with the theoretical results of Matsuoka and Yajima [19].

In this paper, we present experimental results that show evidence of a new mechanism for the compression of the multiple ion-acoustic soliton caused by the velocity change of each pulse of the incident multiple soliton at the reflection point (bottom of the space potential near reflector with deep negative voltage) L_R. The results were as follows. When the initial multiple ion-acoustic soliton is incident obliquely into the sheath area, though the velocity of the first pulse of the multiple soliton hardly changes, each velocity of the second and third pulses is very accelerated just before the reflection point, and decelerated just after it. Consequently, those pulses are compressed by these effects, and become a single soliton. After that, the soliton again becomes a multiple soliton resembling its incident. This appears to be a recurrence phenomenon of a plane soliton. The reflection and/or transmission of the incident soliton, of course, are caused by these velocity changes at the reflection point. Just after compression, second and/or third pulse velocities of the transmitted soliton become much smaller than those of the incident multiple soliton. The velocity ratio (incident pulse velocity to transmitted pulse velocity) depends on the bias voltage on the reflector.

The present paper is organized as follows. The experimental apparatus and plasma parameters are presented in Sec. II, and experimental results on the compressive multiple soliton structure and the reflection and/or transmission coefficient as a function of the velocity ratio of incidence and transmission are given in Sec. III. The experimental and theoretical results are compared in Sec. IV and final results summarized in Sec. V.

II. EXPERIMENTAL APPARATUS

The experiments were carried out in argon plasma at a pressure of $P=(3-4)\times 10^{-4}$ Torr. The plasma was produced in a double-plasma device using multidipole magnets. The typical parameters were as follows: plasma density $n_e = 5\times 10^8$ cm^{-3}; electron temperature $T_e = 2.0-3.7$ eV; and ion temperature $T_i = T_e/(10-12$ eV) measured from the Faraday cup. The geometry of the experimental setup is shown in Fig. 1. The reflector, a copper mesh (350×300 mm^2, 6 mesh/cm, transparency 64%), could be rotated through an angle ($0° < \theta_I < 60°$) around its axis, and be biased at the desired potential V_b with respect to the plasma (floating potential $= -25$ V$< V_b < -500$ V). The axis of the reflector was set at 15 cm from the separation grid of the double plasmas.

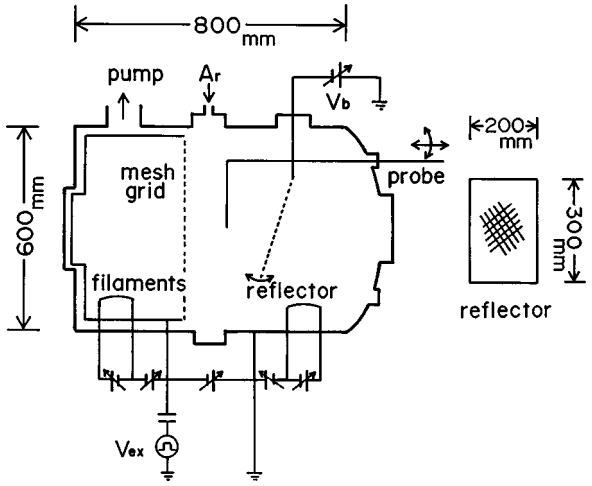

FIG. 1. Schematics of the experimental apparatus.

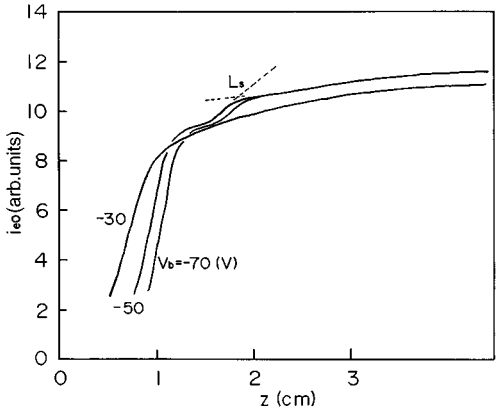

FIG. 2. Profile of the electron saturation current as a function of the distance from the reflector. The reflector is set at $z=0$, incident angle is kept $\theta_I=30°$, V_b is bias voltage on the reflector. $z=L_S$: Point of the sheath edge (z is the distance from the reflector).

III. EXPERIMENTAL RESULTS

The traces of electron saturation current are shown as a function of the distance from the reflector in Fig. 2, and the reflector is biased to a deeper negative voltage than the plasma potential. Here, the bias voltage can be set arbitrarily. As seen from the figure, the electron saturation current decreases greatly near the reflector. We define the ion-sheath edge ($z=L_S$) as the intersection of two tangent lines for rising and/or saturation areas of the electron current I_{e0}. This sheath edge (e.g., $z=L_S\cong 1.8-2.0$ cm, for $V_b=-50$ V, where z is a distance from the reflector on the center of the cylinder and the incident angle is kept constant at $\theta_I=30°$) moves with a negative bias voltage away from the reflector.

The ion-acoustic solitons were picked up with a tiny cylindrical probe (0.1 mm diameter by 1 mm length) on which a slightly positive potential relative to the plasma potential was maintained in order to collect the electron component of the wave. Signals from the probe were displayed on an oscilloscope or analyzed using a boxcar averager. The wave was excited by a double-plasma action by applying a positive pulse with a half of the sinusoidal wave form (pulse width is kept around 10 μsec) to the driver plasma.

Typical wave forms are shown in Fig. 3(a), where I, R_1, R_2, and T are the incident soliton, reflected soliton, reflected wave, and transmitted soliton, respectively. As each pulse of the incident soliton is piled up near the reflection point, the incident multiple soliton is compressed to become a single soliton. After passing through the reflection point, the single soliton again becomes a multiple soliton T, and moves toward the reflector that was biased on the deep negative voltages.

Loci of the maximum amplitude of each pulse of multiple soliton are shown in Fig. 3(b). From this figure we can obtain the velocity of each pulse. As can be seen, when the multiple soliton goes into the reflection point, though the velocity of the first pulse $I_{(1)}$ is hardly changed, the velocities of the second and/or third pulses $I_{(2)}$, $I_{(3)}$ are greatly accelerated just before the reflection point and decelerated just after it. The reflection soliton R_1 is produced at this point. Each pulse which passes through the deceleration area goes toward

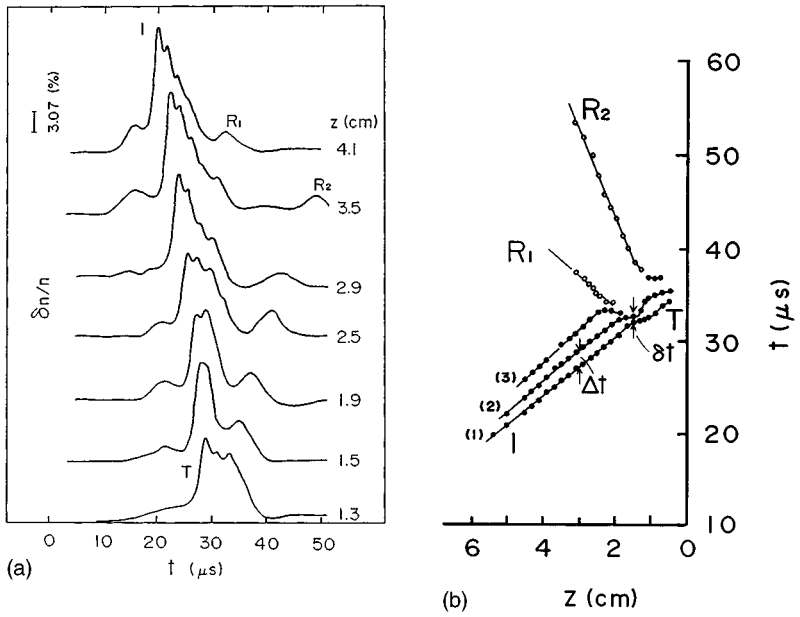

FIG. 3. (a) Typical wave forms of the excited ion-acoustic soliton. I: Incident soliton; T: Transmitted soliton; R_1: Reflected soliton; R_2: Reflected waves. V_b is the floating potential, and $\theta_I=30°$. (b) Loci of the maximum amplitude of each pulse. (1), (2), and (3) are the first, second, and third pulses of the incident soliton, respectively. Δt and δt are time gap of the first and second pulses before the sheath edge ($z>L_S$) and time gap of those at the compression point ($z=L_R$), respectively.

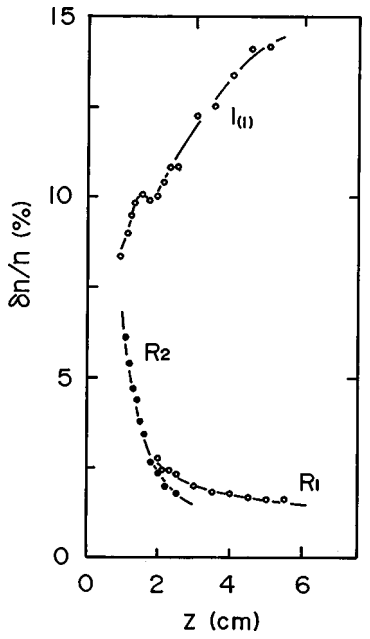

FIG. 4. Amplitude of each wave as a function of the distance z from the reflector. $I_{(1)}$: First pulse of the incident multiple soliton; R_1: Reflected soliton; R_2: Reflected wave. V_b is the floating potential, and $\theta_I = 30°$.

the reflector with large accelerated velocity by deep negative potential on the reflector, and another reflection wave R_2 is produced near the reflector. Here, the velocity of each of the pulses can be represented as $v_{I(1)} \cong v_{I(2)} \cong v_{I(3)} = v_I = (2.7-3.1)\times 10^5$ cm/sec, where $v_{I(1)}$, $v_{I(2)}$, and $v_{I(3)}$ are the velocities of the first, second, and third pulses of the incident multiple soliton and the velocity of R_1 and R_2 is $v_{R1} = (0.94-1.0)v_I$ and $v_{R2} = (0.35-0.41)v_I$, respectively.

Dependence on the z axis (the center of the cylinder) of the maximum amplitude of each wave $(I_{(1)}, R_1, R_2)$ is shown in Fig. 4. The incident multiple soliton goes into the reflection point accompanying decay of the amplitude, but its amplitude increases slightly at the compressed position. The amplitudes of the reflection pulses can be shown empirically as

$$\frac{\delta n(z)}{n} = \kappa z^{-p_i} \quad (i = 1,2), \tag{1}$$

where $p_1 \cong 0.94$ for R_1 and $p_2 \cong 1.6$ for R_2. The amplitude decay of R_2 for z is much larger than that of R_1. Also, although R_1 shows characteristics of a plane soliton [23], the wave width and velocity of R_2 are, respectively, larger and smaller than those of a plane soliton.

The reflection and transmission coefficients γ_R and γ_T are shown in Fig. 5 as a function of the velocity ratio $\alpha_{(2)} = v_{I(2)}/v_{T(2)}$ of the second pulse of the incident multiple soliton. Here, $v_{T(2)}$ is the velocity of the second pulse of the transmitted multiple soliton. The solid lines indicate the theoretical results, which will be discussed later. As seen from the figure, γ_R increases with $\alpha_{(2)}$, and the experimental results are in reasonable agreement with the theoretical ones. γ_T, however, is nearly independent of the velocity ratio, and the experimental values are smaller than the theoretical ones [Eqs. (16) and (17)]. Here, the amplitudes of the first and

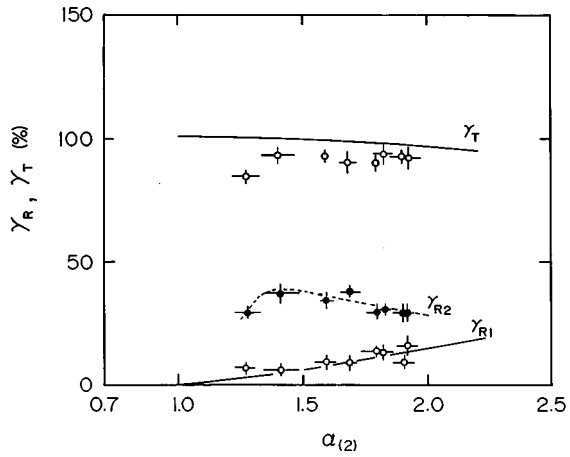

FIG. 5. γ_R and γ_T are the reflection and transmission coefficients as a function of the velocity ratio $\alpha_{(2)}$ of the second pulse, where $\alpha_{(2)} = v_{I(2)}/v_{T(2)}$; $v_{I(2)}$ and $v_{T(2)}$ are velocities of the second pulse of the incident and transmitted multiple solitons, respectively. $\theta_I = 30°$. Solid lines are calculated results from Eqs. (16) and (17).

second pulses of the incident multiple soliton are $\delta n_{I(1)}/n = 15-17\,\%$ and $\delta n_{I(2)}/n = 10-12\,\%$ under these experimental conditions, respectively.

Figure 6 shows the amplitude ratio as a function of the bias voltages on the reflector. Here, $\delta n_p/n$ is the amplitude of the compressed soliton at the reflection point, and $\delta n_{I(1)}/n$ is that of the first pulse just before the sheath edge. The amplitude of the compressed soliton becomes slightly larger than that of the first pulse, and increases with the negatively biased voltages on the reflector.

Each relationship of the velocity ratios $\alpha_{(1)}$ and $\alpha_{(2)}$ for the incident angle θ_I is shown in Fig. 7. The closed and open circles represent, respectively, the experimental results of the first pulse and the second pulse of the incident multiple soliton. The reflection occurs in the hatched area, where the velocity ratio is larger than unity. The solid line for $\alpha_{(2)}$ and the hatched area show the calculated results for Eqs. (7) and (18), respectively, which will be discussed later. We can see in this figure that the velocity ratio $\alpha_{(2)}$ of the second pulse is much larger than the velocity ratio $\alpha_{(1)}$ of the first pulse. When the incident angle increases, the velocity ratio $\alpha_{(2)}$ of the second pulse increases slightly, but $\alpha_{(1)}$ of the first pulse is independent of the incident angle θ_I and maintains its

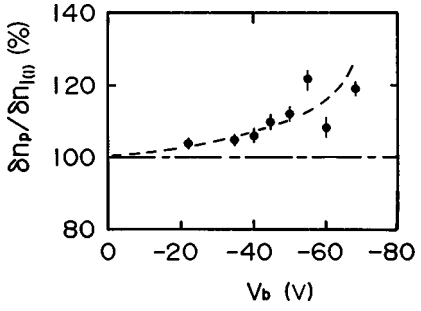

FIG. 6. Amplitude ratio $(\delta n_p/n)/(\delta n_{I(1)}/n)$ as a function of the bias voltages on the reflector V_b, where $\delta n_p/n$ and $\delta n_{I(1)}/n$ are the amplitudes of the compressed soliton at the reflection point and those of the first pulse of the incident soliton, respectively.

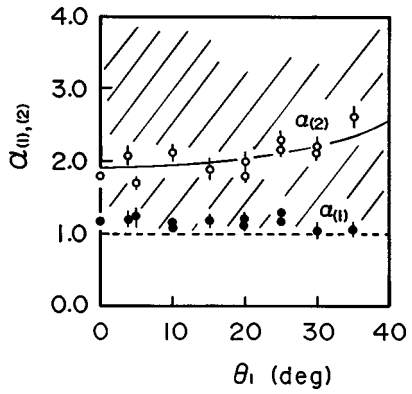

FIG. 7. Each velocity ratio $\alpha_{(1)}$ and $\alpha_{(2)}$ as a function of the incident angle θ_I. Solid line: Calculation result from Eq. (7). Hatched area: Theoretical result given by Eq. (18) and $\alpha_{(2)}>0$. Closed and open circles correspond to the first and second pulses of the incident multiple soliton, respectively.

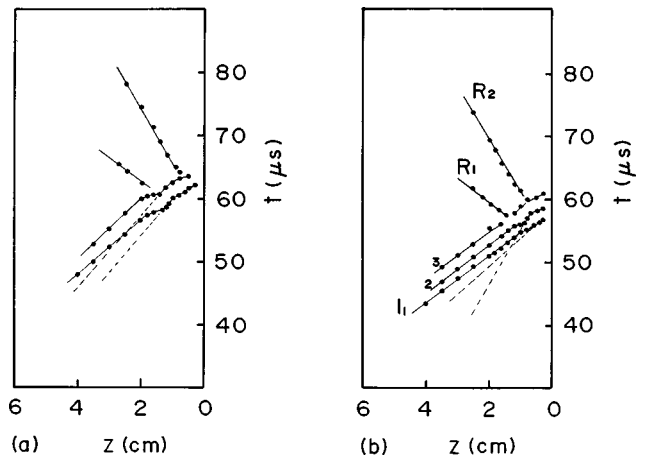

FIG. 8. Loci of each pulse as a function of the distance z from the reflector. V_b is the floating potential, $\theta_I=30°$. Amplitude of the first pulse of the incident soliton is $\delta n_{I(1)}/n\cong$ (a) 6.2, and (b) 14%.

small value ($\alpha_{(1)}\cong 1$). Consequently, the reflection wave R_1 is produced by the velocity change of the second pulse of the incident multiple soliton at the reflection point L_R.

Loci of the solitons are shown in Figs. 8(a) and 8(b). In the experimental conditions of each case, the incident angle and/or bias voltage on the reflector are equal, but the initial soliton amplitude shown in Fig. 8(a) is smaller than that shown in Fig. 8(b). As seen from these figures, when the amplitude of the initial soliton is small, the velocity of the first pulse is changed in equivalence with that of the second pulse at the reflection point, but each velocity ratio of the first and second pulses becomes, respectively, smaller and larger with the amplitude increases, as seen in Fig. 8(b).

Figure 9(a) shows the velocity ratio at the reflection point L_R as a function of the amplitude of the first pulse $\delta n_{I(1)}/n$ of the initial multiple soliton. When the amplitude of the first pulse increases, the velocity ratio $\alpha_{(1)}$ of the first pulse decreases as it approaches $\alpha_{(1)}=1$, while that of the second pulse increases to apparent saturation. These results suggest that when the amplitude of the first pulse is about 5%, both the first- and second-pulse velocities are changed as in Fig. 8(a), and the reflection wave produced by these velocities is also changed. However, when the amplitude becomes larger than 5%, although the change in the velocity of the first pulse is reduced, that of the second pulse becomes larger, and a reflection wave like that in Fig. 8(b) is produced. When the amplitude of the first pulse becomes larger, the nonlinearity becomes stronger [5]. This means that the velocity change and reflection coefficient of the first pulse is decreased, but the velocity ratio $\alpha_{(2)}$ of the second pulse is increased and thereby produces a reflection wave. The velocity ratio is also changed by the bias voltage on the reflector, as seen in Fig. 9(b). In this case, the value of the velocity ratio $\alpha_{(1)}$ of the first pulse at the reflection point L_R remains small ($\alpha_{(1)}\cong 1$), but $\alpha_{(2)}$ of the second pulse becomes larger with the negatively biased voltages on the reflector.

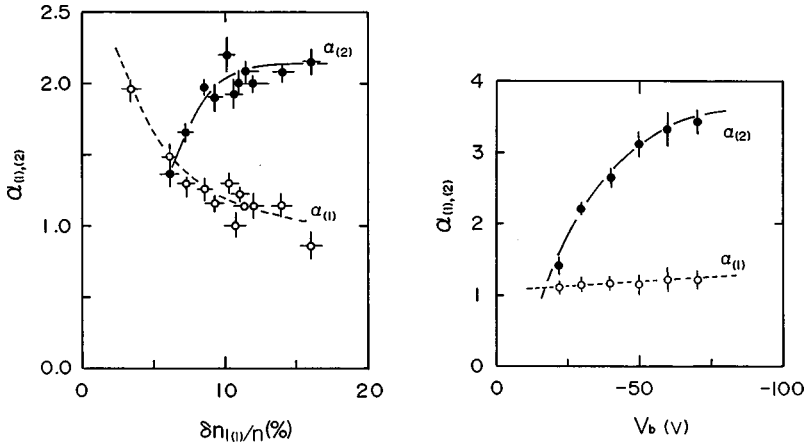

FIG. 9. (a) Each velocity ratio $\alpha_{(1)}$, $\alpha_{(2)}$ as a function of the amplitude of the first pulse of the incident soliton $\delta n_{I(1)}/n$. Open and closed circles correspond to $\alpha_{(1)}=v_{I(1)}/v_{T(1)}$ and $\alpha_{(2)}=v_{I(2)}/v_{T(2)}$, respectively, where $v_{I(1)}$ and $v_{I(2)}$ are velocities of the first and second pulses of the incident multiple soliton, respectively, $v_{T(1)}$ and $v_{T(2)}$ are velocities of the first pulse and the second pulse of the transmitted multiple soliton, respectively. V_b is the floating potential and $\theta_I=30°$. (b) Each velocity ratio $\alpha_{(1)}$, $\alpha_{(2)}$ as a function of the bias voltage on the reflector, V_b. Each pulse amplitude of the incident soliton is kept constant. Incident angle is $\theta_I=30°$. Open and closed circles correspond to $\alpha_{(1)}$ and $\alpha_{(2)}$, respectively.

IV. DISCUSSION

A. The locus of the second pulse of the multiple soliton

Based on the deep negative voltage on the reflector in Fig. 2, we can assume that the electron density n_e and ion density n_i become as shown in Fig. 10(a1), and thus that Poisson's equation becomes $d^2\phi_0(z)/dz^2 = 4\pi e(n_e - n_i) < 0 (L_R < z < L_S), > 0 (L_R < z < L_R), < 0 (0 < z < L_R - D_1)$, and the static space potential $\phi_0(z)$ adopts the shape shown in Fig. 10(a2). Here, the change of $\phi_0(z)$ at $z = L_R$ (reflection point) increases with the negative bias voltage V_b on the reflector. Also, we assume that an ion-wakefield potential [26] $\phi_1(z)$ as shown in Fig. 10(a2) is produced in the area $z > L_R - D_1$ by the first pulse $I_{(1)}$ which behaves like an ion-beam bunch in the area $z < L_R - D_1$ for the deep negative potential on the reflector, where D_1 is the width of the first pulse $I_{(1)}$ of the incident multiple soliton. So $\phi_1(z)$ increases with the incident amplitude $\delta n_{i(1)}/n$ of the first pulse. Consequently, all space potentials are as follows:

$$\phi(z) = \begin{cases} \phi_0(z) & \text{for } I_{(1)} \text{ at } 0 < z < L_R + D_1, \quad \text{for } I_{(2)} \text{ at } L_R < z < L_R + D_1 \\ \phi_0(z) + \phi_1(z) & \text{for } I_{(2)} \text{ at } L_R - D_1 < z < L_R, \quad \text{for } I_{(3)} \text{ at } L_R < z < L_R + D_1 \end{cases} \tag{2}$$

as seen in Figs. 10(a2) and 10(a3). So the second pulse is accelerated at $L_R < z < L_R + D_1$ by the space potential $\phi_0(z)$, and more decelerated at $L_R - D_1 < z < L_R$ by potential $\phi_0(z) + \phi_1(z)$. At the same time, the third pulse $I_{(3)}$ is more accelerated at $L_R < z < L_R + D_1$ by $\phi_0(z) + \phi_1(z)$. Therefore the velocity change of the second pulse at the reflection point L_R increases with both the amplitude of the first pulse $\delta n_{I(1)}/n$ and the negatively biased voltage on the reflector V_b, as seen in Figs. 9(a) and 9(b), respectively. The second pulse is also reflected by this velocity change at the reflection point L_R.

Here, we focus our discussion on the locus of the second pulse from the point of view of the energy conservation law and employing the following particle model:

$$v_{I(2)}^2 = v(z)^2 + \frac{2e\phi(z)}{M}, \tag{3}$$

where $v_{I(2)}$ and $v(z)$ are the velocities of the second pulse at $z > 2$ and $z \leq 2$, respectively, $\phi(z)$ is the space potential at $z \leq 2$, and M is the ion mass. Therefore it is appropriate to place $\phi(z) = \phi_0(z) = -|V_b/\sigma| \sin\{(z - 1.5)\pi/2D_1\}$ eV in area L_1. Here, $V_b = -50$ V and $\sigma = 12.5$ is the best fitting value for the experimental results. Point $z = 1.5$ corresponds to the reflection point $L_R = L_S - D_1$ in this experiment condition, as seen in Fig. 3. Consequently, using Eq. (3), the ion velocity $v(z)$ in area L_1 can be given as

$$v(z)/v_{1(2)} = \sqrt{1 + 1.91 \sin(z - 1.0)\pi/2D_1} \quad (1.5 < z \leq 2.0), \tag{4}$$

where we set $v_{I(2)} = 3.18 \times 10^5$ cm/sec at $z > 2.0$, $D_1 = 0.5$ cm: half-width of the first pulse (soliton), $z = 1.5 = L_R$: reflection point, $z = 2.0 = L_R + D_1$; also set, in area L_2,

$$v(z)/v_{I(2)} = \sqrt{2.91 - 2.61 \sin(z - 1.0)\pi/D_1} \quad (1.0 < z \leq 1.5), \tag{5}$$

where the electron temperature $kT_e = 3.68$ eV and the ion-wakefield potential $|\phi_1(z)| = kT_e \delta n/n = 1.47$ V (amplitude $\delta n/n = 40\%$), such that we arrive at, approximately, $\phi(z) = \phi_0(z) + \phi_1(z) = -(1.47 + |V_b/12.5|)\sin\{(z - 1.0)\pi/D_1\} - |V_b/12.5|$, $V_b = -50$ V; when we set $\phi(z) = \phi_0(z) = V_b e^{-z} = -50e^{-z}$ eV in the area $0 < z \leq 1.0$ [27], the equation

$$v(z)/v_{I(2)} = \sqrt{1 + 23.9e^{-z}} \quad (0 < z \leq 1.0) \tag{6}$$

should be satisfied. In Fig. 10(b), the calculated results of Eqs. (4)–(6) for the locus of the second pulse are shown with solid lines, and closed and open circles show the experimental results for $\theta_I = 30°$ and $V_b = -50$ V.

Also, the width of the sheath area ($0 \leq z \leq L_S$) expands with the incident angle θ_I by the relation $L = L_0/\cos\theta_I$ ($z = L_0$ is the sheath edge for the incident angle $\theta_I = 0°$), so that the acceleration L_1 and/or deceleration area L_2 expands. By these effects, the velocity ratio $\alpha_{(2)}(\theta_I)$ for the second pulse increases with the incident angle θ_I, as shown by the solid line in Fig. 7.

Therefore we think that the rate of the velocity change of the second pulse at the reflection point is proportional to the width of the acceleration and deceleration areas, and we set the velocity ratio of the second pulse as the following function of the incident angle θ_I:

$$\alpha_{(2)}(\theta_I) = \frac{\alpha_{(2)}(0)}{\cos\theta_I} \quad (0° \leq \theta_I \leq 90°). \tag{7}$$

Here, $\alpha_{(2)}(0) = 1.9$ is the value most in agreement with the experimental results.

B. Calculation of the reflection and/or transmission coefficients from the conservation laws of momentum and/or energy in a plane system

The plane soliton is shown by the equation

$$a = A \operatorname{sech}^2(Kz - \Omega t), \tag{8}$$

where A is an amplitude and K and Ω are the characteristic wave number and frequency, respectively. The momentum $|\mathbf{P}| = P$ and energy E of the plain soliton may be given as

$$P = \int A \operatorname{sech}^2(Kz - \Omega t)dz = \sqrt{6A}, \tag{9}$$

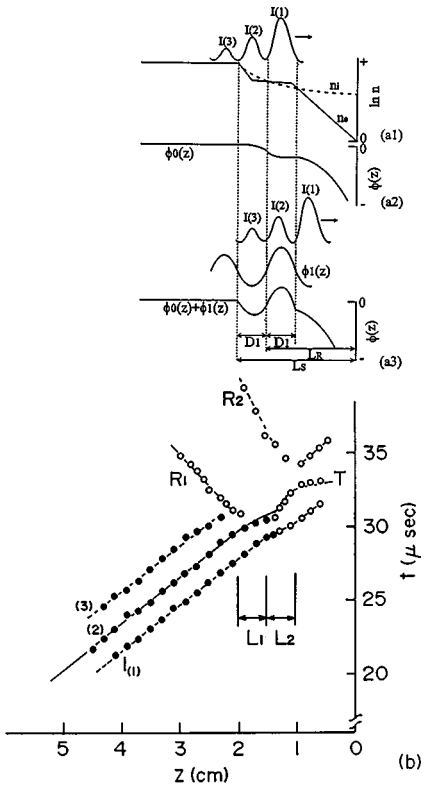

FIG. 10. (a1), (a2) Schematics of the space potential $\phi(z)$ and/or incident soliton I. $\phi_0(z)$ is the static space potential, $\phi_1(z)$ is the ion-wakefield potential. L_R: Reflection point. D_1: Soliton width of the first pulse of the incident soliton. (b) Solid line is the calculated results of Eqs. (4)–(6). Closed circles are experimental results, and incident angle is $\theta_I=30°$, and bias potential is $V_b=-50$ V. L_1: Acceleration area; L_2: Deceleration area ($L_1=L_2=D_1$). L_S: Point of the sheath edge; L_R: Reflection point.

$$E=\int A^2\ \mathrm{sech}^4(Kz-\Omega t)dz=\sqrt{6A^3}. \tag{10}$$

Here, we applied a soliton's character $AD^2=6$. Now, the conservation of the momentum and/or energy of the solitons consisting of the incident soliton (I), reflected soliton (R), and transmitted soliton (T) can be written as

$$P_I=P_R+P_T, \tag{11}$$

$$E_I=E_R+E_T. \tag{12}$$

From Eqs. (9) and (11) the parallel and perpendicular components of the momentum to the reflector surface $P_\parallel$ and $P_\perp$, are given as

$$\sqrt{A_I}\sin\theta_I=\sqrt{A_T}\sin\theta_T+\sqrt{A_R}\sin\theta_R, \quad P_\parallel, \tag{13}$$

$$\sqrt{A_I}\cos\theta_I=\sqrt{A_T}\cos\theta_T-\sqrt{A_R}\cos\theta_R, \quad P_\perp, \tag{14}$$

where A_I, A_R, and A_T are the maximum amplitude of the incident soliton, of the reflected soliton, and of the transmitted soliton, respectively, and where θ_I, θ_R, and θ_T are the incident angle, reflection angle, and transmission angle, respectively.

Also, we can arrive at the following equation by Snell's law:

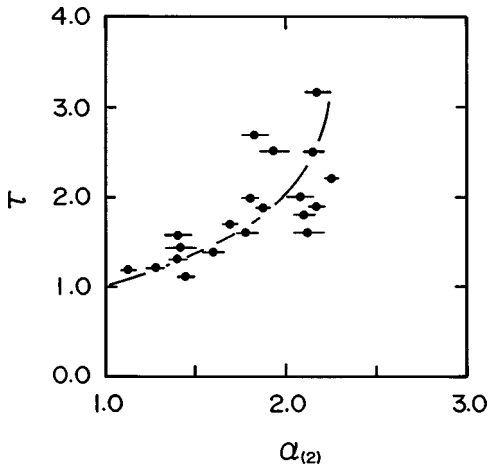

FIG. 11. Intensity $\tau=\Delta t/\delta t$ of the coupling of the first and second pulses as a function of the velocity ratio $\alpha_{(2)}$ of the second pulse. Δt and δt are the time gap of the first and second pulses before the sheath edge and at the compression point, respectively.

$$\sin\theta_T=\frac{\sin\theta_I}{\alpha_{(2)}}, \quad \alpha_{(2)}=\frac{v_{I(2)}}{v_{T(2)}}, \quad 0<\theta_I,\theta_T<\frac{\pi}{2}, \tag{15}$$

where v_I and v_T are the velocities of the incident and transmitted solitons, respectively, and where it is assumed that $\sin\theta_I\cong\sin\theta_R$.

The reflection coefficient $\gamma_R=A_R/A_I$ is defined by using Eqs. (13)–(15) as follows:

$$\left(\frac{A_R}{A_I}\right)^{1/2}=\gamma_R^{1/2}=\frac{\sqrt{1-(\sin t\theta_I/\alpha_{(2)})^2}-\cos\theta_I/\alpha_{(2)}}{\sqrt{1-(\sin\theta_I/\alpha_{(2)})^2}+\cos\theta_I/\alpha_{(2)}}. \tag{16}$$

Also, from Eqs. (10) and (12), the transmission coefficient $\gamma_T=A_T/A_I$ is given as

$$\gamma_T=(1-\gamma_R^{3/2})^{2/3}. \tag{17}$$

Consequently, γ_R and γ_T are dependent on the incident angle and the velocity ratio of the second pulse.

Here, the condition of the reflection is given by Eq. (16) as

$$\sqrt{1-(\sin\theta_I/\alpha_{(2)})^2}-(\cos\theta_I/\alpha_{(2)})>0. \tag{18}$$

Consequently, we can take $\alpha_{(2)}>1$ from Eq. (18), where $\alpha_{(2)}>0$. The hatched area in Fig. 7 shows these results.

C. Compressive phenomena at the reflection point

The velocity of the first pulse of the incident multiple soliton with large amplitude is hardly changed just before the reflection point L_R, but velocities of the second and/or third pulses are more accelerated by the uneven space potential $\phi(z)=\phi_0(z)+\phi_1(z)$ as seen in Fig. 10(a3). Consequently, each pulse of the incident multiple soliton is piled up at the reflection point, its soliton is compressed, and a single soliton is shaped.

Next, we introduce the relation

$$\tau = \frac{\Delta t}{\delta t}. \tag{19}$$

Here, τ shows the intensity of the coupling of the first and second pulses at the reflection point, and it is shown as a function of the velocity ratio $\alpha_{(2)}$ of the second pulse in Fig. 11. As can be seen from this figure, τ increases with the velocity ratio. That is, compression of the first and second pulses becomes strong with the velocity ratio of the second pulse.

V. CONCLUSION

When the multiple soliton propagates obliquely towards the reflector that is biased to deep negative potential, the velocities of the second and/or third pulses are accelerated just before the reflection point ($z > L_R$), and decelerated just after it ($z < L_R$) by the uneven space potential that is produced by both the deep negative voltage on the reflector and an ion wakefield. By these effects, each pulse of the incident multiple soliton is piled up and compressed at the reflection point, but the velocity of the first pulse hardly changes at the reflection point. After passing through the reflection point, it again assumes the form of a multiple soliton, much as the incident soliton does. This result is similar to the recurrence phenomenon, except that it is compulsory and dependent on an external condition, that is, it is different from the self-recurrence of the KdV-type soliton. Also, the reflection and transmitted solitons are produced at the reflection point, and these amplitudes are dependent on the velocity ratio of the second pulse of the incident multiple soliton.

Finally, the velocity ratio of the incident and transmitted solitons depends on the bias voltages on the reflector and on the amplitude of the incident multiple soliton.

ACKNOWLEDGMENT

A portion of the present work was supported by a Grant-in Aid for Scientific Research from the Ministry of Education, Science and Culture, Japan.

[1] N. J. Zabusky and M. D. Kruskal, Phys. Rev. Lett. **15**, 34 (1965).
[2] H. Ikezi, Phys. Fluids **16**, 1668 (1973).
[3] S. Watanabe, O. Ishihara, and H. Tanaka, Plasma Phys. **17**, 345 (1975).
[4] Y. Nishida, T. Nagasawa, and S. Kawamata, Phys. Rev. Lett. **42**, 379 (1979).
[5] T. Nagasawa and Y. Nishida, Plasma Phys. **23**, 575 (1981).
[6] Y. Nishida and T. Nagasawa, Phys. Rev. Lett. **45**, 1626 (1981).
[7] T. Nagasawa and Y. Nishida, Phys. Rev. A **28**, 3043 (1983).
[8] I. Alexeff and R. V. Neidigh, Phys. Rev. Lett. **7**, 223 (1961).
[9] L. Schott, Phys. Fluids **26**, 3431 (1983); **29**, 846 (1986).
[10] W. D. Jones and I. Alexeff, in *Proceedings of the 7th International Conference on Phenomena in Ionized Gases*, edited by B. Perovic and D. Tosic (Grade-vinska Knjiga, Belgrade, 1966), Vol. 2, p. 330.
[11] P. D. Golden and W. M. Leavens, Phys. Fluids **13**, 433 (1970).
[12] R. P. Dahiya, P. I. John, and Y. C. Saxena, Phys. Lett. **65A**, 119 (1977).
[13] Y. Nishida, Phys. Fluids **27**, 2176 (1984).
[14] Y. Nakamura, T. Nomura, and T. Itoh, in Proceedings of the International Conference on Plasma Physics, Nagoya, 1980 (unpublished).
[15] S. Raychaudhuri, H. Y. Chang, E. K. Tsikis, and K. E. Lonngren, Phys. Fluids **28**, 2125 (1985).
[16] O. Ishihara, I. Alexeff, H. J. Doucet, and W. D. Jones, Phys. Fluids **21**, 2211 (1978).
[17] I. Ibrahim and H. H. Kuehl, Phys. Fluids **27**, 962 (1984).
[18] K. Imen and H. H. Kuehl, Phys. Fluids **30**, 73 (1987).
[19] C. Matsuoka and N. Yajima, J. Phys. Soc. Jpn. **58**, 3939 (1989).
[20] T. Nagasawa and Y. Nishida, Phys. Rev. Lett. **56**, 2688 (1986).
[21] Y. Nishida, K. Yoshida, and T. Nagasawa, Phys. Lett. A **131**, 83 (1988).
[22] T. Nagasawa, K. Yoshida, and Y. Nishida, 1989 International Conference on Plasma Physics, New Delhi, India, edited by A. Sen and P. K. Kaw (unpublished).
[23] T. Nagasawa and Y. Nishida, Phys. Lett. A **162**, 278 (1992).
[24] T. Nagasawa and Y. Nishida, 1992 International Conference on Plasma Physics, Innsbruck, 1992, edited by W. Freysinger, K. Lackner, R. Schrittwieser, and W. Lindinger (unpublished).
[25] T. Nagasawa and Y. Nishida, Phys. Rev. E **49**, 4442 (1994).
[26] Y. Nishida, T. Okazaki, N. Yugami, and T. Nagasawa, Phys. Rev. Lett. **66**, 2328 (1991).
[27] Y. Nishida, K. Yoshida, and T. Nagasawa, Phys. Fluids B **5**, 722 (1993).